Extensional rupture of model non-Newtonian fluid filaments

Joel Koplik
Benjamin Levich Institute and Department of Physics, City College of the City University of New York, New York, New York 10031

Jayanth R. Banavar
Department of Physics, The Pennsylvania State University, University Park, Pennsylvania 16802

(Received 30 July 2002; published 10 January 2003)

We present molecular dynamics computer simulations of filaments of a model non-Newtonian liquid stretched in a uniaxial deformation to the point of breaking. The liquid consists of Lennard-Jones monomers bound into chains of 100 monomers by nonlinear springs, and several different constant-velocity and constant-strain-rate deformations are considered. Generally we observe nonuniform extensions originating in an interplay between the stretching forces and elastic and capillary restoring mechanisms, leading to highly uneven shapes and alternating stretched and unstretched regions of liquid. Except at the fastest pulling speeds, the filaments continue to thin indefinitely and break only when depleted of molecules, rather than due to common viscoelastic rupture mechanisms.

DOI: 10.1103/PhysRevE.67.011502 PACS number(s): 83.50.−v, 61.25.Hq, 47.55.Dz, 47.20.Dr

I. INTRODUCTION

The extensional dynamics of polymeric, non-Newtonian liquids controls processes ranging from commonplace activities such as chewing gum to large-scale commercial applications in extrusion processing of materials [1]. Understanding the dynamics of the liquid in these situations [2] requires information beyond the usual shear viscosity characterization of flowing fluids, and has led to extensive experimental and theoretical work on ''liquid bridges'' [3]. Here, one pulls on the ends of a cylinder of the liquid and observes shapes, forces, velocities, and (to some degree) stresses, and attempts to relate the behavior to an appropriate rheological model. The ultimate fate of an extending liquid bridge is a rupture at some point, and some efforts in this direction have attempted to understand the fracture mechanisms involved. Aside from practical relevance to material failure, the thinning dynamics of a cylindrical neck of liquid has become an important subject in fluid interfacial dynamics [4]. In almost all cases, these efforts have concerned macroscopic bodies of liquid, in the sense that the experiments do not generally have atomic resolution, and the calculations are based on continuum descriptions. The purpose of this paper is to consider the interfacial rupture of a liquid bridge configuration at an atomic scale. In addition to the intellectual question of exploring the late stages of rupture that are below the level of resolution considered previously, a further motivation comes from recent interest in microfluidics and nanofluidics [5], where precisely these length and time scales can be reached in practice.

The focus of this paper is somewhat outside the domain usually considered in rheology. Previous studies of the rupture of liquid filaments [6] have concentrated on determining instability criteria based on continuum modeling, focusing on identifying characteristic regions of the strain rate – maximum strain phase space corresponding to viscous, elastic, rubbery, and glassy behavior. In that context it is common to distinguish a recoverable or elastic component of the strain, representing the residual deformation of the material when the stretching forces are released and it is allowed to retract, as opposed to an irrecoverable part due to viscous dissipation or structural alteration. For example [7], it is claimed based on an analysis of experimental data that in some flow regimes true rupture occurs only when the recoverable strain exceeds 1/2. In the systems studied here, this approach is difficult to apply, since it neglects an important (elastic) component, surface tension, which tends to restore all distorted but unconstrained liquid bodies to a spherical shape. Furthermore, it is difficult to keep track of dissipation in the simulations reported here because the thermostat used to maintain a fixed temperature constantly adds or subtracts energy from the system. A second focus of previous work has been the relation between time to rupture and applied stress; in our simulations the ends of the filament are moved at prescribed velocities, so that applied stress is not fixed and instead fluctuates during the course of the stretch. To discuss other configurations, empirical correlations or the results of non-Newtonian continuum modeling are used. The simulations performed here quickly lead to regions of the filament which are only a few molecules in diameter, and not obviously described in these ways.

We have previously considered the rupture of fluid interfaces in two situations, using molecular dynamics (MD) simulations. In a study of the dynamics of a monatomic drop placed in a second immiscible fluid undergoing shear [8], we found fair quantitative agreement with experiments and continuum calculations in general, and in particular that the drop ruptures at a sufficiently large capillary number. The microscopic mechanism involved is a gradual flow of the drop's molecules to one side or another induced by the external flow, coupled to surface tension (originating in the molecular interactions chosen to provide immiscibility) acting to reduce the area of the interface separating the drop and solvent liquids. In a previous paper on non-Newtonian fluids [10] we used MD simulations to study liquid bridge deformation, focusing on the shape evolution and internal velocity and stress fields. In that paper relatively small samples of several different model molecular fluids were considered—a Newton-

 ©2003 The American Physical Society

ian liquid based on short-chain molecules, a solution of a few longer (20–40 monomers) molecules in a short-chain solvent, and melts of the longer chains. Although the simulations were continued to the point of rupture, these systems were too small to display any interesting behavior that could be quantitatively analyzed. The Newtonian liquid and melt systems ruptured due to fracture after only modest length increases, by less than a factor of 2. The model solution system attained rather longer lengths, by virtue of the longer molecules becoming extended and providing a kind of backbone, and ruptured when the overall length exceeded the amount of molecular backbone available, essentially following the monatomic mechanism. Our goal here is to use a larger system based on a melt of longer molecules, and study the deformations of highly elongated liquid filaments.

II. SIMULATION PROCEDURE

The simulational method and the molecular system closely follows our earlier papers on nanodrop dynamics [9], liquid bridge extensional flows [10], and single chains in a flow [11]. The MD calculations themselves are of standard form [12,13], and consider a fluid made of monomers interacting with two-body forces of two types, a Lennard-Jones potential to provide an impenetrable core and chemical attraction at larger distances, along with a finitely extensible nonlinear elastic force to link the monomers into model polymer chains. The explicit forms of the interaction potentials are

$$V_{\mathrm{LJ}}(r)=4\epsilon\left[\left(\frac{r}{\sigma}\right)^{-12}-\left(\frac{r}{\sigma}\right)^{-6}\right],$$

$$V_{\mathrm{FENE}}(r)=-\frac{1}{2}kr_0^2\ln\left(1-\frac{r^2}{r_0^2}\right). \tag{1}$$

The Lennard-Jones (LJ) interaction acts between any two monomers separated by a distance less than $r_c=2.5\sigma$, and a linear term is added to V_{LJ} so that the force vanishes at this cutoff. The finitely extensible nonlinear elastic (FENE) potential [2] acts only between adjoining monomers in any one molecule, and has the effect of limiting the bond length to r_0. The parameters in the FENE potential are taken to be $r_0=1.5\sigma$ and $k=30\epsilon/\sigma^2$, following Kremer and Grest [14], and are chosen to yield an entangled melt of noncrossing chains for the 100-monomer chain length used here. The characteristic time for monomer dynamics is defined by the LJ parameters, $\tau=\sqrt{\epsilon/m\sigma^2}$, where m is the monomer mass. In the remainder of this paper, and in particular in all figures, when dimensions are not given we have implicitly nondimensionalized using ''MD units,'' where σ is the unit of length, τ is the unit of time, and ϵ is the unit of energy.

A molecular liquid based on the FENE and LJ potentials (1) has been widely studied as an MD model of polymer melts [15]. In most previous work, the 6-12 potential is cut off at a smaller value than used here, $r_c=2^{1/6}\sigma$, which has the computational advantage of reducing the number of particles that are in interaction range and speeding the calculation. The properties of this system are given in detail in Ref. [16]. This value of r_c corresponds to a purely repulsive potential, which, while adequate for a confined material, has the disadvantage here that a fluid will expand to fill space uniformly, with no interface. Since an interface is crucial here, attraction is needed and we retain the larger value of r_c. However, because the interaction has been altered, the liquid studied here need not have the same transport coefficients. In separate simulations we find a static shear viscosity $\mu(0)\sim 10^3 m/\sigma\tau$, defined as the limit of the dynamic shear viscosity $\mu(\dot{\gamma})$, the ratio of shear stress to strain rate in Couette flow, when the strain rate tends to zero. Typically, polymer melts based on LJ and FENE potentials show shear thinning—a nearly constant viscosity up to a certain transition shear rate $\dot{\gamma}^*$, and a systematic (roughly power-law) decrease at larger values. We use the inverse of the transition shear rate as a characteristic fluid relaxation time, $\lambda\equiv 1/\dot{\gamma}^*\sim 10^5\tau$ in this case. This number and the quoted viscosity above are very crude estimates: at the very low velocities needed to reach the plateau for this chain length, the signal-to-noise ratio in a stress measurement is poor, and even in very long runs, substantial fluctuations are found. The rheology of chain liquids and the definition of characteristic time in this context is discussed further in Refs. [16,10]; the latter paper considers MD simulations of the liquid bridge extensional dynamics of model melts (and other fluids) and also shows that they exhibit strain hardening in extensional flow, in the sense that an appropriate extensional viscosity increases with strain rate. Finally, the surface tension is measured to be $\alpha=0.37\pm 0.01$ using an independent equilibrium simulation of a slab of liquid with planar interfaces [17].

The MD calculations are performed in parallel on either T-3E, Origin-3000, or IBM SP platforms, using a spatial domain decomposition algorithm, a layered linked-cell list on each processor, and message passing interface (MPI) routines. The numerical procedure is to integrate Newton's equations of motion using the velocity Verlet algorithm [12] with time step 0.005τ. Occasionally, the computation was checked by rerunning over a certain time interval with a smaller step length. A Nosé-Hoover thermostat [18] is used to maintain the liquid at a constant temperature $T=1.5\epsilon/k_B$. The initial configuration, a roughly circular cylinder of length $L_0=80.5\sigma$ and radius $R_0=26.3\sigma$, containing 1400 chain molecules 100 monomers in length, is in a disordered liquid state resulting from a somewhat convoluted preparation procedure. In our earlier simulations of length-100 chain molecule melts [9], we began with the monomers on regular lattice sites and randomized the configuration by heating it at a high temperature and low density in a box with repulsive walls. This system was equilibrated to the point where its time-averaged monomer spatial density was uniform, the probability distributions of molecular sizes (end-to-end length and radius of gyration) reached a steady state, and the probability distributions of molecular orientations were rotationally invariant. A spherical drop was formed by cooling the liquid gradually to temperature 1.5, while simultaneously applying a weak central force until a stable sphere formed, and then gradually switching off the force. Next, half of the sphere was placed on a partially wetting atomistic

TABLE I. Final length and time to rupture (MD units).

	Constant velocity			Constant strain rate		
v_0 or $\dot{\epsilon}_0$	0.05	0.15	0.5	0.001	0.004	0.01
Length	432	694	1080	701	1594	959
Time	3520	2045	1000	2250	763	263

solid substrate and reequilibrated, and finally the sphere was allowed to coalesce with a slightly randomized copy of itself. Because both hemispheres were placed on attracting substrates, the result was a liquid cylinder held between two solid surfaces, rather than a single larger sphere. Removing the solid substrate after coalescence gives the initial cylinder considered here. One might be concerned that when the cylinder is pulled it would tend to break at the midplane into its two original drops due to incomplete healing, but in fact we observe rupture at various other locations.

To stretch the filament, we simply pull on its ends. More precisely, each monomer in a disk of thickness 5σ at each end is attached to a ''tether site'' by a stiff spring, and the tethers are moved outwards in a prescribed manner by displacing their position by the appropriate axial amount $\pm v_0 \Delta t \hat{z}$ at each time step. In simulations of constant-velocity extension, v_0 is just the velocity at each end of the filament, while for constant-strain-rate extension, where the length of the filament grows as $L(t)=L_0 e^{\dot{\epsilon}_0 t}$, the fixed control parameter is the strain rate $\dot{\epsilon}_0$ and the velocity is $v_0(t) = dL(t)/dt$. This procedure is similar to a common experimental one [3], where the liquid filament rests between solid end plates that are moved apart, but has the conveniences that the end plates need not be modeled and that flow along the end plates does not arise. The focus of this paper is the behavior of the liquid in the ''middle'' of the filament, so nothing is lost in this way. We also attempted an alternative procedure suggested by experiments on single DNA molecules [19] in which a constant axial force was applied to each monomer in the end regions, but the result was that the end regions contracted radially and rupture occurred nearby, leaving the bulk of the filament unextended.

The operating conditions of the various simulations performed here are listed in Table I, in terms of the pulling velocity or strain rate. Note that in either case the initial velocity and strain rate are related by $v_0 = L_0 \dot{\epsilon}_0$, where L_0 is the filament's initial length. In terms of the usual dimensionless groups characterizing a flow, at the start of a run the Reynolds number $\mathrm{Re} = \rho v_0 R_0 / \mu(0)$ is always much less than unity, while the Deborah number $\mathrm{De} = \lambda \dot{\epsilon}_0$ and the capillary number $\mathrm{Ca} = \mu(0) v_0 / \alpha$ are $O(10^2)$ or larger. Although the Reynolds, Deborah, and capillary numbers describing this flow are all moderate by laboratory standards, it should be kept in mind that the physical velocities are relatively large, few meters to hundreds of meters per second (depending on one's interpretation of the Lennard-Jones monomers), and not at all small for the microscopically thin bodies of liquid considered here.

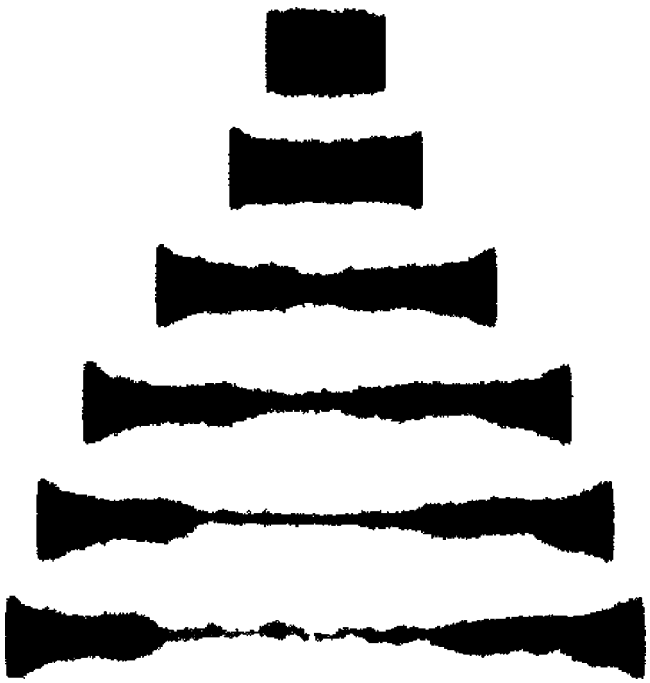

FIG. 1. Sequence of filament shapes in a constant-velocity deformation at pulling speed $v_0 = 0.05\sigma/\tau$, at times 0, 500τ, 1500τ, 2500τ, 3100τ, and 3520τ (top to bottom).

III. CONSTANT-VELOCITY STRETCHING

We first consider filament stretching at a relatively low constant velocity, displacing the two ends at $\pm 0.05\sigma/\tau$. Successive snapshots of the filament appear in Fig. 1, in a low-resolution side view intended to indicate the overall shape. At early times there is a mostly uniform deformation, aside from some necking near the two ends, which results from the tethering method used here—the monomers there are essentially pinned to their initial relative positions and when these are moved apart the melt attempts to fill in. A ''dynamical'' necking down appears near the center of the filament around 1500τ, followed by relatively uniform stretching of the central neck region through 3100τ, while the two end segments of the filament translate with the tethers with only minor changes of shape. Eventually the filament breaks when the neck region is so stretched as to run out of molecules. As seen in the close-up views in Fig. 2, the neck eventually thins down to a few molecular chains lined up along the stretch axis, and the breakage occurs when these chains are pulled in opposite directions and slide past each other. Note that the molecular model used here does not incorporate chain breaking, so the molecular ''depletion'' seen here is the only available rupture mechanism.

Calculations and laboratory experiments [4,20,21] on the thinning of a continuum Newtonian liquid cylinder typically find a power-law variation of minimum radius with time. Here, however, while we do observe a systematic decrease as seen in Fig. 3, the detailed time variation is not well fit by a power of time. Aside from the fact that the later stages of rupture are associated with a neck made of just a small number of highly extended molecules, which may not suffice to form a continuum, the velocities and stresses at the ends of

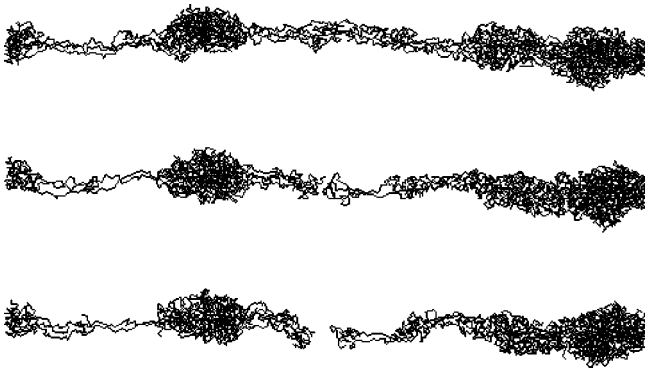

FIG. 2. Rupture region in the constant-velocity deformation of Fig. 1, at times 3475τ, 3515τ, and 3520τ (top to bottom).

the sample show strong relative temporal fluctuations, which are unavoidable in small systems but not present in theoretical calculations or well-designed experiments. Furthermore, at this stage the liquid is presumably highly viscoelastic so that Newtonian fluid predictions may not be applicable at all. It is not therefore unreasonable to observe quantitatively different thinning dynamics. Similar behavior is observed in all of the other cases presented below: although there is a systematic decrease in the filaments' minimum radius with time, it does not fit a power-law variation.

The global behavior of the shape of the filament is of course coupled to the evolution of the typical configurations of the molecules. Individual molecules exhibit a range of behaviors, from becoming fully elongated to remaining coiled up, with only a partial correlation between the initial position in the liquid cylinder and the final state, so instead we focus on statistical averages. In Fig. 4, we show the time dependence of the mean molecule size, defined by the end-to-end molecular length, and the mean orientation, defined by the angle between the end-to-end vector of a molecule and the stretch axis. (Other measures of size and direction, such as the radius of gyration and the orientation of the eigenvectors of the inertia tensor, respectively, exhibit identical trends to those plotted here.) As the filament begins to stretch, an average molecule elongates and aligns with the axis to a modest degree, 15–25 % or so, but after 1500τ the trend reverses and it begins to relax back to its equilibrium length. Orientational relaxation is slower, an obvious effect in the reptation picture, since a chain can easily contract by withdrawal along its axis but must displace other chains to rotate. The transition correlates with the visual behavior of the filament in Fig. 1—after time 1500τ the two ends of the filament, which contain most of its molecules, do not experience any significant extension, and merely translate with little change, in shape while relaxing internally after the initial step in stress. To verify this contention, we consider the molecular configuration as a function of location along the axis. Figure 5(a) shows the length and orientation as a function of axial position at an early time, before the development of the stagnant end regions, and we see that, except for those molecules at the very ends of the filament (which are wholly or partially tethered and have a restricted ability to change shape), there is a roughly uniform extension and

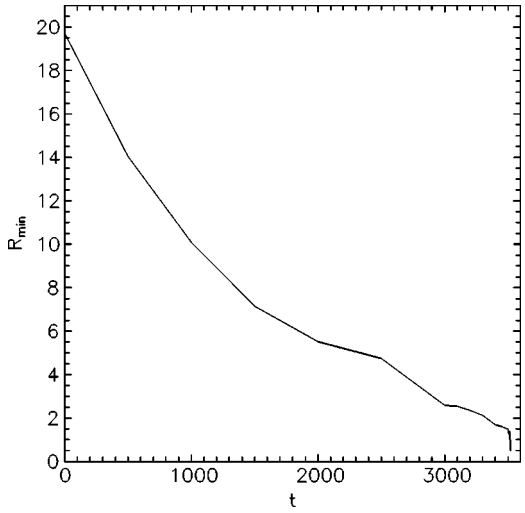

FIG. 3. Minimum radius vs time in the constant-velocity deformation of Fig. 1.

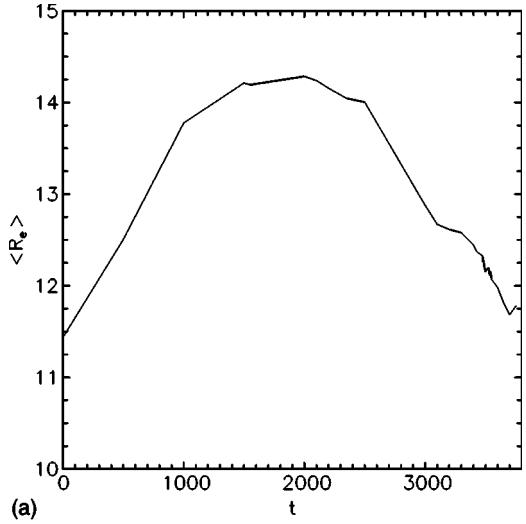

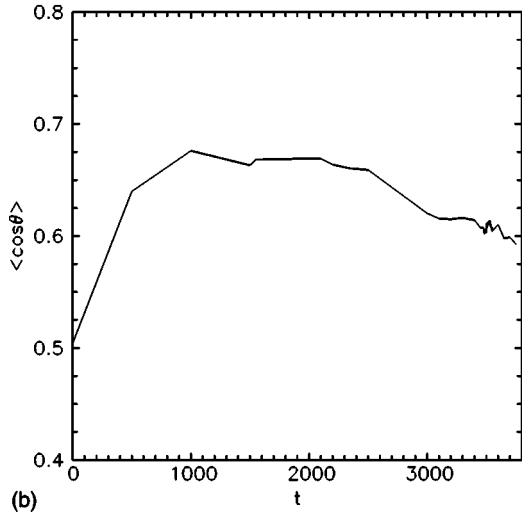

FIG. 4. Mean molecular end-to-end length and orientation angle vs time in the constant-velocity deformation of Fig. 1.

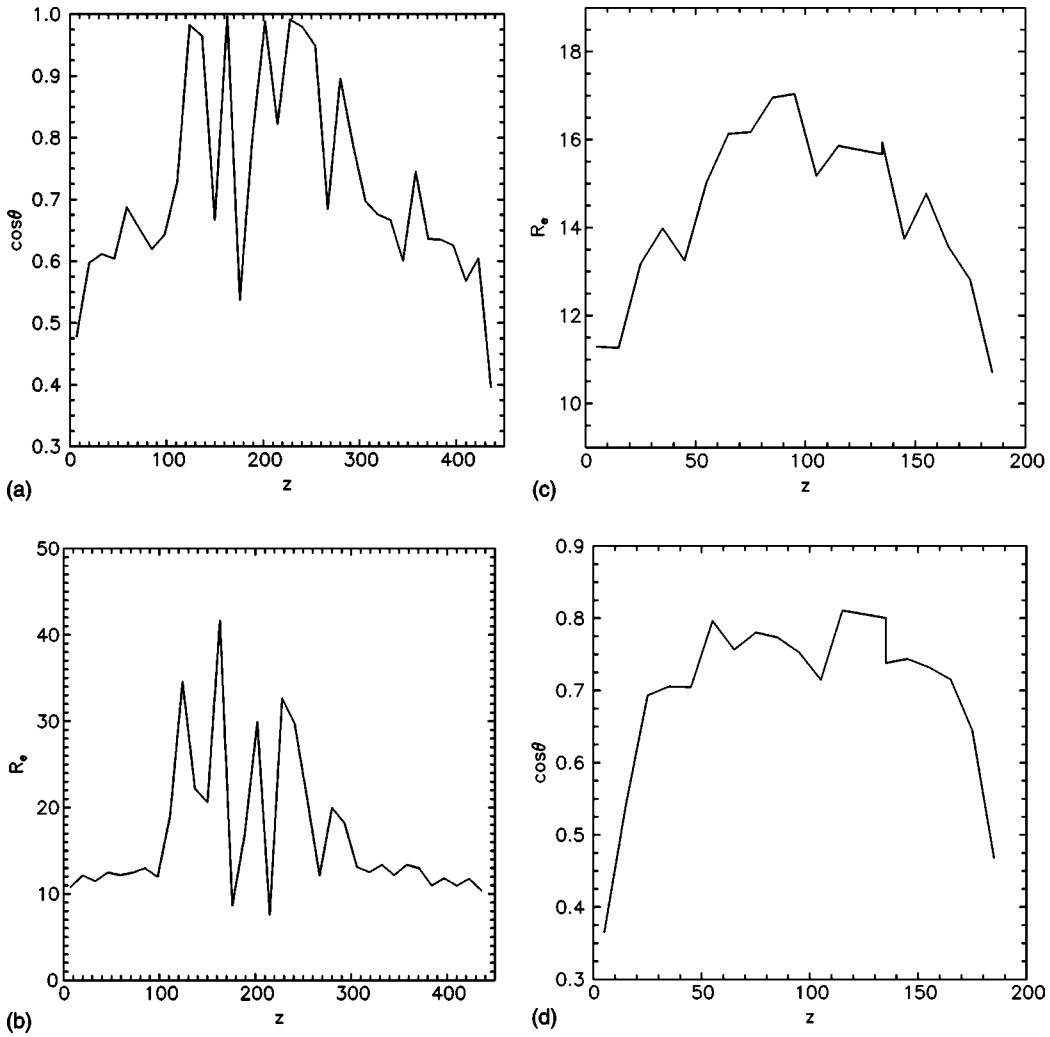

FIG. 5. Molecular length and molecular orientation vs axial position in the constant-velocity deformation of Fig. 1. Top: at time 1000τ, bottom at time 3500τ.

alignment. In contrast, at the late time 3000τ in Fig. 5(b), the prominent configurational changes are confined to the central region, with little elongation elsewhere. Furthermore, in the central region itself there is a rapid variation along the axis from highly stretched to little-stretched intervals. Again this behavior is reflected in the overall shape—the blown-up figures of the central region show an alternation between stretched chains and apparently knotted clusters.

Turning to the continuum flow fields, Fig. 6 gives the fluid velocity as a function of axial position at various times, with behavior consistent with the previous discussion. In the early stages of deformation, when the filament is nearly cylindrical, the velocity varies roughly uniformly along the axis. At intermediate times, there are stagnant end regions moving with the tethers, and a rapid velocity variation in the center. In the last frame, just before rupture, the region near the center where the break will occur is almost at rest, with high-velocity regions to either side, and a bit of an overshoot on the left. The stress tensor measurements are unfortunately rather noisy, as shown in Fig. 7. Generally, the origin of the fluctuations is that the stress depends on the intermolecular forces, which, given the potentials used, are very rapidly varying functions of the particle positions. It is possible to ameliorate the fluctuations using comoving sampling bins and interpolative smoothing methods, and in Ref. [10] we have presented and discussed these in detail for thicker filaments whose behavior more closely resembles continuum properties. Here, we just show an example of the raw data, averaged radially and over short spatial intervals along the axis. The qualitative aspects of the stress may be understood as reflecting features evident in the shape of the filament in this time interval (at 2500τ, as shown in the third frame of Fig. 1), and the general trends seen here as well as in the other simulations described below as are follows.

(1) Positive peaks in the pressure at points where fluid is moving away as the filament thins out.

(2) A radial stress (rr component) that is very noisy but negative, reflecting the radial compression of the filament, and largest in magnitude near the center.

(3) An axial stress that is positive and comparatively noiseless, with peaks at the same points as the pressure.

(4) A noisy shear stress, which on average ramps from negative to positive from end to end, reflecting increasing radial velocity as one moves away from the midplane.

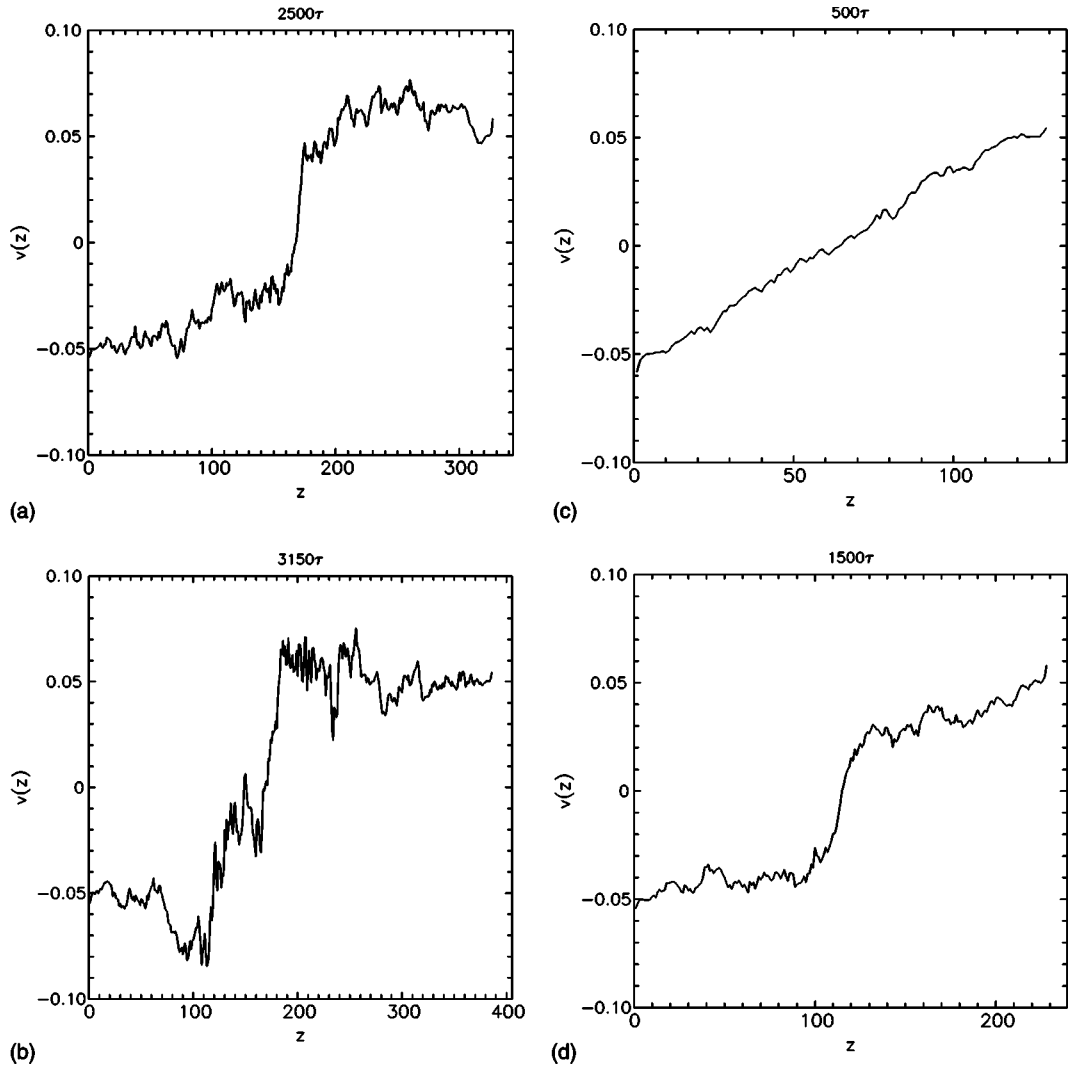

FIG. 6. Velocity vs axial position in the constant-velocity deformation of Fig. 1 at the times indicated. Each curve represents a 50τ time average.

(5) The amount of noise and fluctuation increases over time, reflecting both an increase in the number of thinning and stretching regions and a smaller sample of monomers in each.

Finally, we examine the behavior as a function of stretching velocity. Figures 8 and 9 show a sequence of snapshots at higher (fixed) tether speeds, ± 0.15 and $\pm 0.5\sigma/\tau$, respectively. In these various simulations, the initial liquid cylinder is always the same, and within each sequence the same length scale is used. First note that the rupture occurs at different points along the filament, indicating that the process is random and an indirect function of the particular sequence of fluctuating positions and velocities in each case and, furthermore, that there is no special defect associated with the sample preparation. At these higher speeds, the stagnant end regions do not develop, and more molecules are available to the central portion of the filament, allowing it to attain longer strains before rupture. Here the ends are steadily drawn out, leaving a central region that does expand but at a distinctly slower speed, and begins to evolve into isolated drops. In the central region, relatively rapid thinning occurs at several intermediate points, and the configuration prior to rupture resembles the results of the quasistatic Rayleigh instability [8], where a cylinder of liquid without imposed flow breaks up into spherical drops. The final stages of rupture, again, amount to a very narrow neck, only a few molecules in width, attenuating down to nothing as its elongated chains are pulled past each other. The shape evolution is in a sense opposite to that of the low-velocity case in Fig. 1, where the end regions begin to translate passively before becoming highly stretched. Finally, as indicated in Table I, note that the maximum length attained before breakup increases with pulling speed, while the time to rupture decreases, presumably because the higher stress allows more molecules to be stretched.

IV. CONSTANT-STRAIN-RATE STRETCHING

The more common experimental protocol in liquid bridge systems is stretching at constant strain rate, $\dot{\epsilon}_0 = \dot{L}(t)/L(t)$, leading to an exponential increase in length and velocity. Ostensibly, the motivation is to provide a ''constant-strain

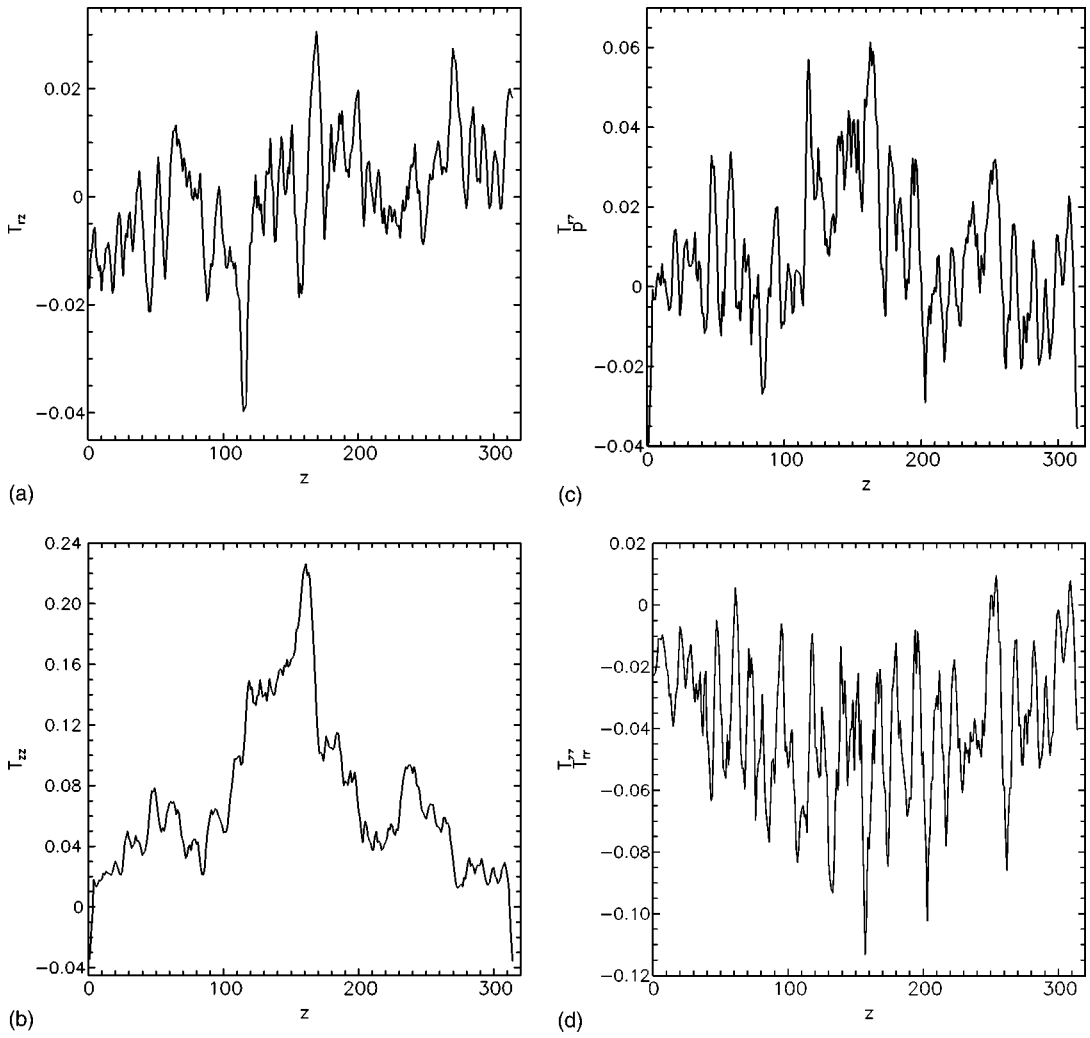

FIG. 7. Stress tensor components vs axial position in the constant-velocity deformation of Fig. 1 at time 2500τ. Clockwise from upper left: pressure (p), radial (rr), axial (zz), and shear (rz) stress.

environment'' for the liquid, to facilitate study of its extensional rheology, although in practice [3,10] the strain can often be very unevenly distributed. In Fig. 10 we show some of the time sequence of shapes observed at a strain rate $\dot{\epsilon}_0 = 0.001\tau^{-1}$. The evolution combines features of the various constant velocity deformations presented above: the filament narrows in the center and eventually ruptures there due to attenuation of molecules, but at the same time the end re-

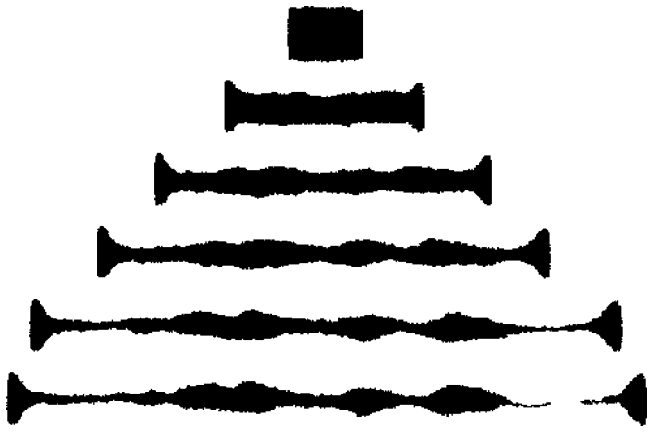

FIG. 8. Sequence of filament shapes in a constant-velocity deformation at pulling speed $v_0 = 0.15\sigma/\tau$, at times 0, 450τ, 950τ, 1770τ, 1870τ, and 2045τ.

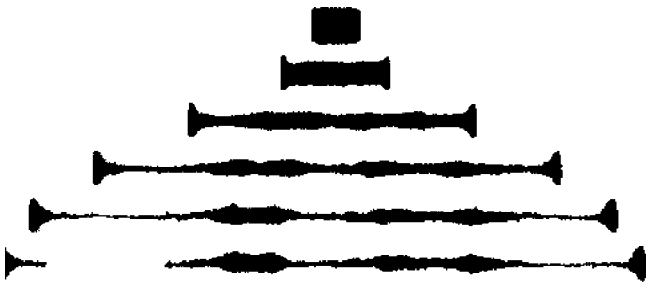

FIG. 9. Sequence of filament shapes in a constant-velocity deformation at pulling speed $v_0 = 0.5\sigma/\tau$, at times 0, 100τ, 400τ, 700τ, 900τ, and 1000τ.

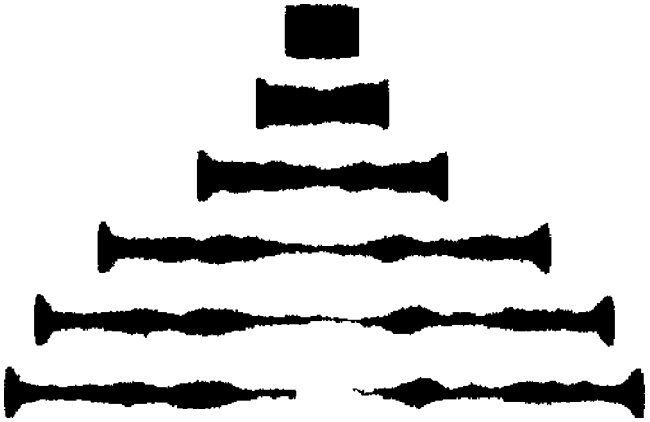

FIG. 10. Sequence of filament shapes in a constant-strain-rate deformation at $\dot{\epsilon}_0 = 0.001\tau^{-1}$, at times 0, 650τ, 1300τ, 1950τ, 2150τ, and 2250τ.

gions are not translating stagnantly, but rather stretch at a slower rate than the bulk, and at the time of rupture are themselves in the process of thinning and presumably would eventually break up due to the Rayleigh instability.

The distinction between constant-velocity and constant-strain deformations is that in the former case the strain rate (and stress) decreases with time, so that after an initial stage where the system is pulled out of its equilibrium configuration, the molecules can relax back; see Fig. 4. In the present case, the stress is ostensibly constant, and the molecules are increasingly elongated and oriented with no configurational relaxation until nearly the time of rupture, as shown in Fig. 11. The behavior of the velocity profiles is also consistent with these remarks; as seen in Fig. 12, the velocity is closer to a linear variation along the axis for a considerably longer time interval.

A somewhat related MD study [22] of the elongation and relaxation of a model polymer melt considered chains of 30 monomers using the same interactions as in this paper (but with a short $r_c = 2^{1/6}\sigma$ LJ cutoff). Instead of simulating the explicit stretching of filaments, a nonequilibrium MD method was used to apply a constant-strain uniaxial elongation to a homogeneous system in a box. Among other things, the behavior of the chain size (radius of gyration) and orientation was measured, and the qualitative behavior is similar to that seen here. The elongation and degree of orientation increased monotonically during the flow, at a rate which increased monotonically with the strain rate, and then relaxed monotonically when the flow was turned off.

We have briefly considered the question of recoverable strain [6] in this simulation, by releasing the tethered monomers after rupture and allowing the liquid to take up a new equilibrium shape without external stress. If the filament is released well before rupture, it seems to withdraw into a sphere, whereas if released just before rupture, the thinning neck continues to thin, rupture occurs anyway, and afterwards the liquid appears to be withdrawing into two spheres. Here the phrase ''appears to be'' means that as a function of time the liquid shape is tending towards one or two spheres at the original liquid density, but the process is so slow that we have not followed it all the way to equilibrium. Similar

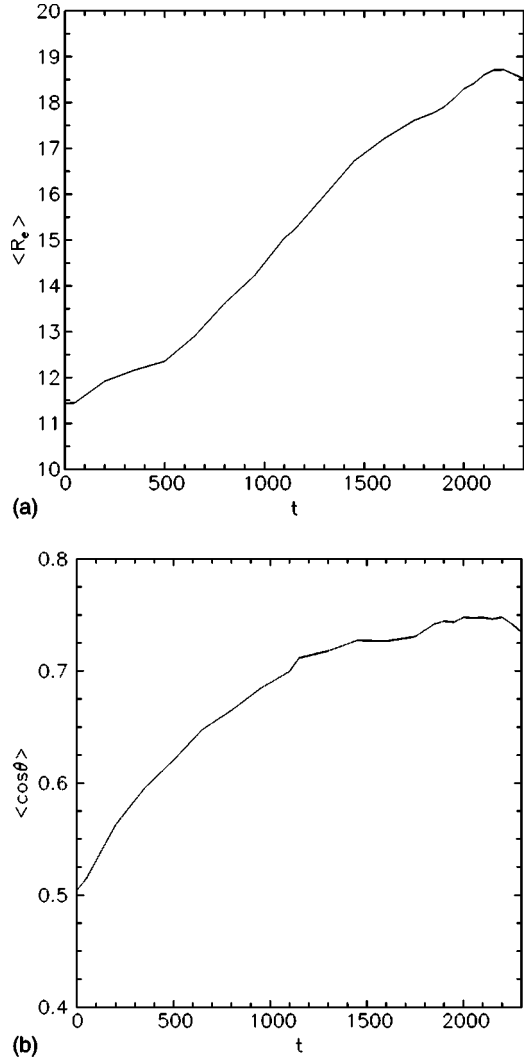

FIG. 11. Mean molecular end-to-end length and orientation angle vs time in the constant-strain deformation of Fig. 10.

behavior is found in the other cases as well. Given that the initial simulated filament was prepared by an equilibration procedure involving the relaxation of a dilute high-temperature melt, it is difficult to see how the final state here would differ in any statistically significant way, other than perhaps the time needed to reach it.

At higher strain rates a different behavior appears, a cohesive failure of the melt in the region where the molecules are tethered to pulling sites. In Fig. 13, at the strain rate $\dot{\epsilon}_0 = 0.004$, there is a rapid thinning at the ends of the filament leaving a central stagnant region showing the onset of a Rayleigh instability, while the thin necks attaching this region to the ends attenuate until breakup. At the same time, some of the tethered molecules are pulled out of the filament, and the fluid bodies at the ends have not had time to relax to an equilibrium shape. At the still higher strain rate $\dot{\epsilon}_0 = 0.01$ shown in Fig. 14, the tethered molecules are simply pulled free of the rest of the filament, and rapid rupture occurs. The rupture times and lengths for the various cases are recorded in Table I.

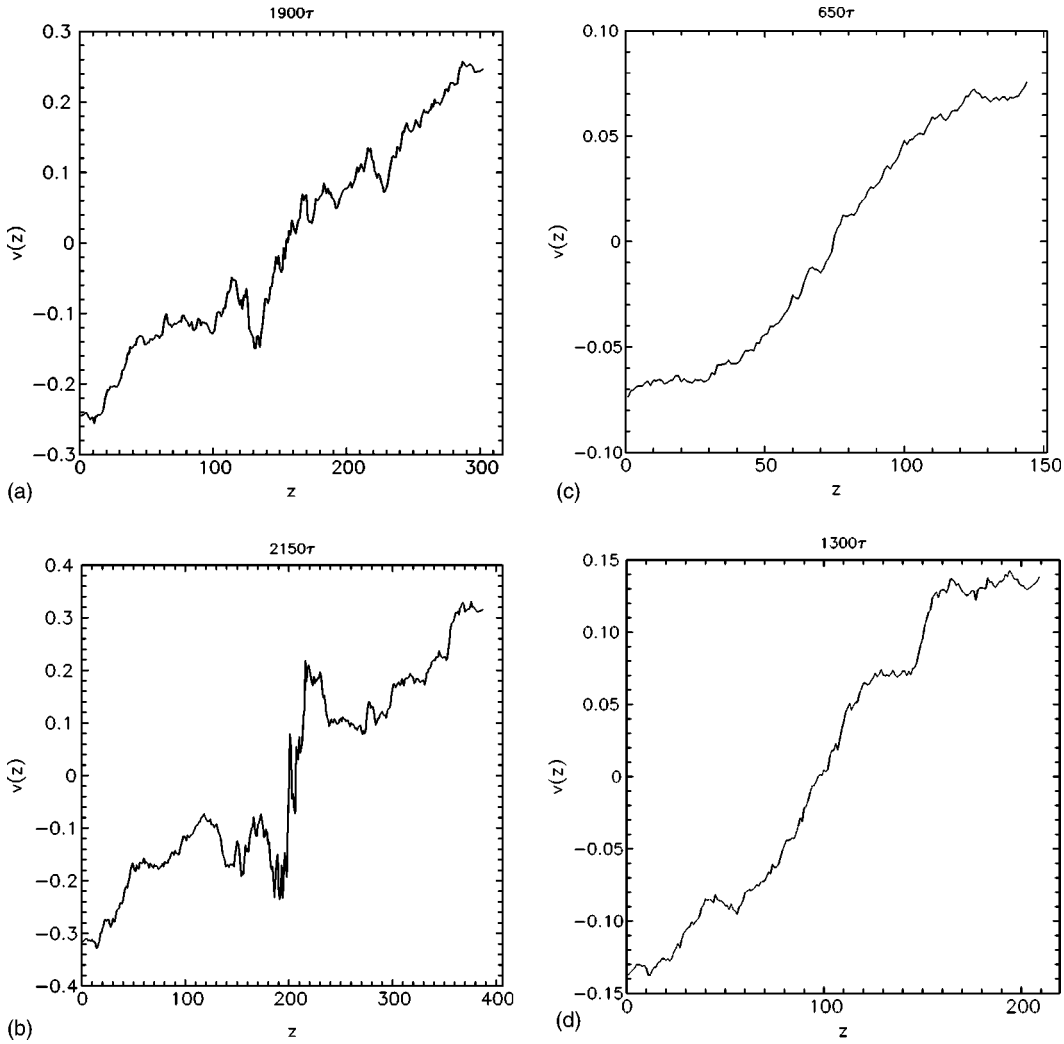

FIG. 12. Velocity vs axial position in the constant-velocity deformation of Fig. 10 at the times indicated. Each curve represents a 50τ time average.

V. FORCE MEASUREMENTS

As an alternative to the stress fields, we have studied the forces from a more direct viewpoint on the monomer scale. The quantity of perhaps most direct experimental relevance is the pulling force exerted on the tethers at the ends. While this quantity is easy to evaluate in the simulations, it is unfortunately quite noisy. Aside from the problem noted above of large atomic-level force fluctuations, in general, here the procedure used to generate the motion exacerbates the problem. The atoms at the ends of the filament are attached to moving tether sites by stiff springs, whose force is very sensitive to small atomic displacements.

In the constant-velocity simulations the result is simple—the pulling force is roughly constant in time, fluctuating about a value which is approximately linearly proportional to the pulling velocity. At the three velocities studied, 0.05,

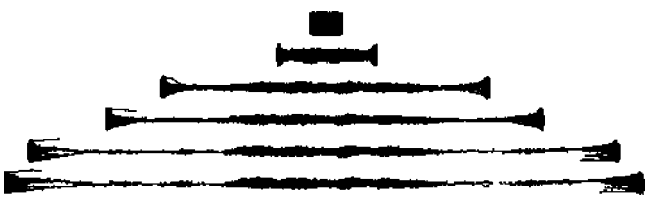

FIG. 13. Sequence of filament shapes in a constant-strain-rate deformation at $\dot{\epsilon}_0 = 0.004\tau^{-1}$, at times 0, 295τ, 595τ, 668τ, 743τ, and 763τ.

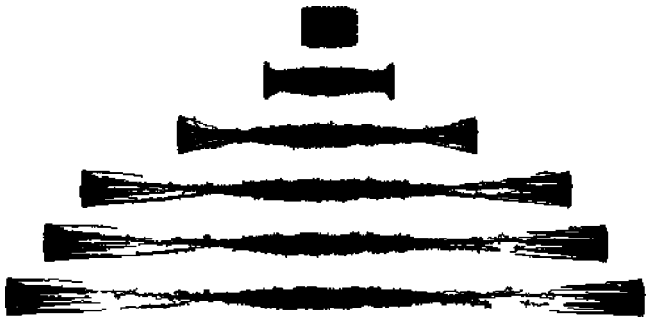

FIG. 14. Sequence of filament shapes in a constant-strain-rate deformation at $\dot{\epsilon}_0 = 0.01\tau^{-1}$, at times 0, 90τ, 175τ, 225τ, 240τ, and 253τ.

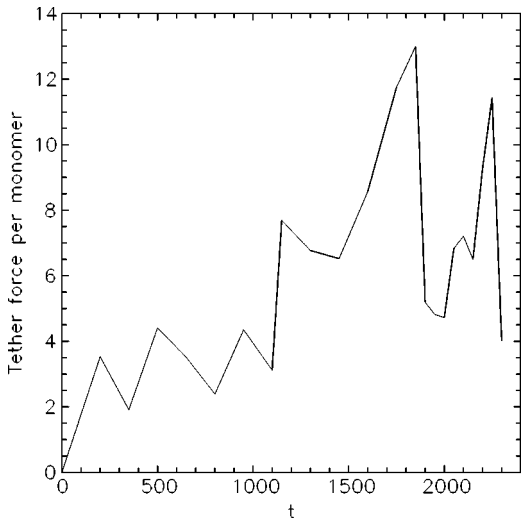

FIG. 15. Variation of the tether force with time in the simulation shown in Fig. 10.

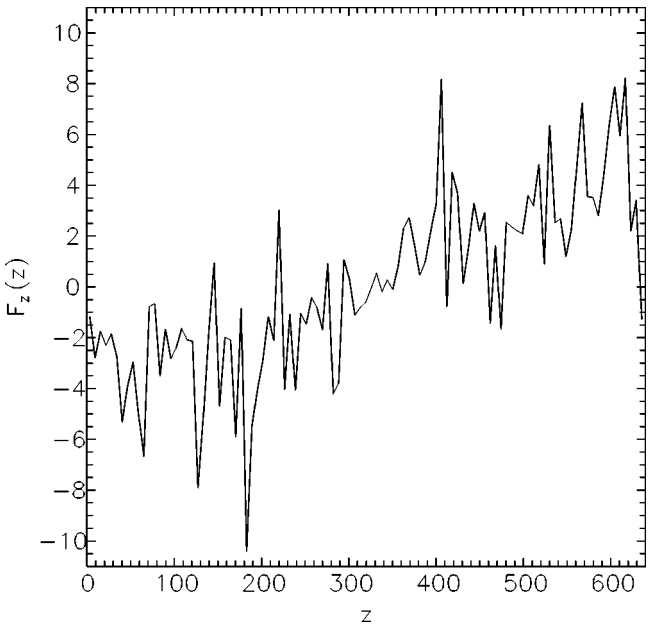

FIG. 16. Axial force as a function of axial position in the filament shown in Fig. 10, at time 2150τ.

0.15, and $0.5\sigma/\tau$, the force per pulled monomer is measured to be 2.72 ± 0.16, 7.31 ± 0.24, and $24.9\pm0.25\epsilon/\sigma$, respectively. [Typical values of the instantaneous force on a monomer at this density and temperature are $O(1-10)$ in this unit, while its time-averaged values over a 100τ interval are an order of magnitude smaller.] One can rationalize the time constancy of the force by arguing that in this case the molecules are moving past each other with a roughly fixed value of relative velocity, and since the material is a viscous liquid in a low Reynolds number flow, there is a constant drag force on each molecule.

In contrast, in the constant-strain-rate cases there is a nontrivial time variation. For example, as shown in Fig. 15 for the lowest rate $\dot{\epsilon}_0=0.001\tau^{-1}$, the tether force jumps to a finite value once the force is applied, then increases with time until about 1750τ. After a sharp drop, the force again increases until rupture. Referring to Fig. 10, after this transition time the right and left sides of the filament are approximately translating without a significant shape change, while the central region thins down to nothing. The early increase can then be associated with strain hardening [3,10] and the shape deformation of the entire liquid filament, the sharp drop with relaxation of stress after some internal readjustment and formation of the central neck, the second increase with the strain hardening of the central thinner region, and the final dropoff with rupture. At the next highest strain value, $0.004\tau^{-1}$, the numerical values of the tether force are comparable, and the tether force shows a similar variation, with a corresponding drop at about 600τ, the time at which (see Fig. 13) the central region of the filament halts and ceases to change its shape while the regions to either side continue to elongate. At still higher strain rates there is no obvious pattern to the tether force evolution; the fragmentation of the regions near the tethers makes it difficult to identify simple mechanisms.

We can also compute the forces in the interior of the filament, and in Fig. 16 we show an example of the force in the axial direction in the $\epsilon_0=0.001$ constant-strain-rate simulation at time 2150τ, averaged over a 100τ time interval and a 6σ spatial interval along the axis. The force on the end regions containing the tethered monomer shows large spatial and temporal fluctuations for the reasons given at the beginning of this section, and these two regions have been suppressed in this plot. Aside from the fluctuations, the trend is a roughly linear ramp with positive (negative) values corresponding to the halves of the filament moving to the right (left). As a function of time, the fluctuations shift around apparently randomly, and the height of the ramp is roughly constant in time. At higher strain rates, the analogous plot is again a fluctuating quasilinear ramp in its central region, but shows rapid spatial fluctuations near the ends, corresponding to molecules being pulled out there. In contrast, in the constant-velocity simulations there is always a linear ramp as a function of z and, furthermore, at different pulling speeds the ramp height is roughly linear in velocity.

VI. CONCLUSIONS

We have discussed the results of molecular simulations of a liquid filament of a model polymer melt stretched to the point of rupture. These model systems are composed of nonbreakable, freely jointed, entangled chains, and the rupture process typically involves ductile failure of some sort. Here we observed these filaments stretch into a very nonuniform shape, with one or more thin necked regions, and then fail when one of the necks simply attenuates down to nothing. More precisely, during the stretching process the thinning neck regions are populated with well-extended chain molecules lying roughly parallel to the extension axis, which are drawn past each other to one side or the other by their respective interacting neighbors. Eventually the filament is held together by only a few such adjacent elongated chains, and splits once these slide past each other. In analogous ear-

lier simulations in systems of melts or solutions based on shorter length molecules (up to 20 monomers), presumably unentangled, a more familiar form of ductile fracture was observed, in which a neck several molecules in thickness separated into two pieces [10]. In that case, a model solution was able to attain the longest lengths prior to breakup, and there one could see that the fully extended longer molecules acted as a backbone that stiffened the filament, and breakage occurred when the filament was extended to the point where these backbone molecules were no longer in contact with each other.

In continuum terms, the neck thins under a combination of mass transfer due to outflow and (Rayleigh) capillary instability. The outflow, in an idealized unidirectional flow situation, would lead to a filament thinning uniformly and exponentially in time, at a rate controlled by the imposed end velocities, whereas realistic fluid mechanical calculations [4] give power-law thinning rates, whose scale is again fixed by the external stretching rate and a nonconstant but monotonic radius variation along the axis near the rupture point. The Rayleigh instability is present with or without flow, and originates in the fact that a fixed volume liquid cylinder reduces its surface area by breaking up into spheres, and is driven by surface tension while viscosity resists the flow. In general, both mechanisms are present and one expects Rayleigh instabilities to be important at low pulling speeds, while thinning (or other mechanisms such as a fracture) should dominate at higher velocities. In the present simulations thinning is always the rupture mechanism, because the late stages always resemble Fig. 2, but signs of incipient capillary instability are always present as well. The growth rate of the fastest instability mode for a continuum Newtonian liquid otherwise at rest is approximately [24] $\alpha/6R\mu(0) \sim 10^{-5}\tau^{-1}$ here, somewhat smaller than observed in the simulations, and again any number of factors could account for the discrepancy.

In terms of the classification of failure zones by Malkin and Petrie [6], the constant velocity and lowest-rate constant-strain runs are in the ''flow zone,'' where viscous deformation can proceed indefinitely, provided there is enough liquid. The two runs at higher constant strain appear to have ''glassy states,'' at least near the tethers where rupture occurs.

The filament shapes observed here seem unusually irregular compared to those studied elsewhere, and in no case do we observe a long neck of nearly constant diameter. Note, however, that these simulations begin with a liquid sample whose diameter is already in the nanometer range, and so these results should at best be compared to the last, usually poorly-quantified stages of typical laboratory studies. The surface irregularities and fluctuations are, however, quite characteristic of molecular simulations of moving microscopic liquid bodies with free surfaces [8,23]. As a consequence of these fluctuations, the measured continuum fields show sufficiently large statistical fluctuations as to be nontrivial to understand even qualitatively. Even microscopic measurements that do yield a smooth result, such as the variation of minimum filament radius with time, are not in agreement with continuum calculations. The molecular level information is likewise fluctuating, but does seems to be readily interpretable at this scale.

Another issue in comparing these results to laboratory measurements is the pulling speed involved. Although the standard dimensionless groups characterizing these flows, the Reynolds, Deborah, and capillary numbers, are similar to those considered elsewhere, there is quite a difference in velocities. In typical liquid flows, the drift or peculiar velocity is a small fraction of the thermal velocity of the monomers, but here, particularly in the late stages of the constant-strain simulations, the tether velocity approaches the thermal velocity, $O(1\sigma/\tau)$. The severe fragmentation of the end regions of the filament is presumably one aspect of this high speed, but a second is that surface tension effects, which would ordinarily smooth a free surface, may not have time to act.

ACKNOWLEDGMENTS

We thank M. M. Denn for discussions, the NASA Office of Physical and Biological Sciences for financial support, and the NASA Advanced Supercomputing Division at the Ames Research Center and NPACI at the San Diego Supercomputer Center for providing computational resources.

[1] R. I. Tanner, *Engineering Rheology*, 2nd ed. (Oxford, New York, 2000); N. G. McCrum, C. P. Buckley, and C. B. Bucknall, *Principles of Polymer Engineering*, 2nd ed. (Oxford, New York, 1997).

[2] R. B. Bird, C. F. Curtiss, R. C. Armstrong, and O. Hassager, *Dynamics of Polymeric Liquids*, 2nd ed. (Wiley, New York, 1987), Vol. 2.

[3] G.H. McKinley and T. Sridhar, Annu. Rev. Fluid Mech. **34**, 375 (2002).

[4] J. Eggers, Rev. Mod. Phys. **69**, 865 (1997).

[5] C.-M. Ho and Y.-C. Tai, Annu. Rev. Fluid Mech. **30**, 579 (1998); G. E. Karniadakis and A. Beskok, *Micro Flows: Fundamentals and Simulation* (Springer, New York, 2002).

[6] A recent discussion with extensive references is A.Ya. Malkin and C.J.S. Petrie, J. Rheol. **41**, 1 (1997).

[7] G.V. Vinogradov, Rheol. Acta **14**, 942 (1975).

[8] J. Koplik and J.R. Banavar, Phys. Fluids A **5**, 521 (1993).

[9] J. Koplik, S. Pal, and J.R. Banavar, Phys. Rev. E **65**, 021504 (2002).

[10] B. Busic, J. Koplik, and J. R. Banavar, J. Non-Newtonian Fluid Mech. (to be published).

[11] M. Cheon, I. Chang, J. Koplik, and J.R. Banavar, Europhys. Lett. **58**, 215 (2002).

[12] M. P. Allen and D. J. Tildesley, *Computer Simulation of Liquids* (Clarendon Press, Oxford, 1987).

[13] J. Koplik and J.R. Banavar, Annu. Rev. Fluid Mech. **27**, 257 (1995).

[14] K. Kremer and G.S. Grest, J. Chem. Phys. **92**, 5057 (1990). This paper deduced an entanglement length of 35, while more recent work [M. Putz, K. Kremer, and G.S. Grest, Europhys.

Lett. **49**, 735 (2000)] gives a revised estimate of 70.
[15] *Monte Carlo and Molecular Dynamics Simulations in Polymer Science*, edited by K. Binder (Oxford, New York, 1995).
[16] M. Kröger, W. Loose, and S. Hess, J. Rheol. **37**, 1057 (1993).
[17] J. S. Rowlinson and B. Widom, *Molecular Theory of Capillarity* (Oxford University Press, Oxford, 1982).
[18] S. Nosé, Mol. Phys. **52**, 255 (1984); W.G. Hoover, Phys. Rev. A **31**, 1695 (1985).
[19] S.B. Smith, L. Finzi, and C. Bustamante, Science **258**, 1122 (1992).
[20] I. Cohen and S.R. Nagle, Phys. Fluids **13**, 3533 (2001).
[21] A.U. Chen, P.K. Notz, and O.A. Basaran, Phys. Rev. Lett. **88**, 174501 (2002).
[22] M. Kröger, C. Luap, and R. Muller, Macromolecules **30**, 526 (1997).
[23] M. Moesler and U. Landman, Science **289**, 1165 (2000).
[24] Lord Rayleigh, Philos. Mag. **34**, 145 (1892).